# AIAA 2000-0823

## Further Investigation of a Higher-Order Algorithm for Aerodynamic Computations

S. De Rango, and D.W. Zingg
*Institute for Aerospace Studies*
*University of Toronto*
*Toronto, Ontario, Canada*

**38th Aerospace Sciences Meeting & Exhibit**
10-13 January 2000/Reno, NV

# Further Investigation of a Higher-Order Algorithm for Aerodynamic Computations

S. De Rango,*and D.W. Zingg†
*Institute for Aerospace Studies*
*University of Toronto*
*Toronto, Ontario, Canada*

**A higher-order spatial discretization is presented for the solution of the thin-layer Navier-Stokes equations with application to two-dimensional turbulent aerodynamic flows. The discretization of the inviscid and viscous fluxes and the turbulence model, the numerical boundary schemes, and the numerical integration technique used to calculate forces and moments have all been raised to a level of accuracy consistent with third-order global accuracy. Systematic grid convergence studies are used to determine the numerical error for several subsonic and transonic test cases on a variety of grids. These studies show that the higher-order algorithm produces highly accurate solutions even on relatively coarse grids. Comparisons with a well-established second-order algorithm demonstrate that significant savings in computing expense can be achieved using the higher-order discretization.**

## Introduction

The potential of higher-order methods (which we define to be methods of order three or greater) to reduce the cost of numerical solutions of hyperbolic partial differential equations has been recognized for a long time.[1,2] In applications requiring high accuracy, such as direct simulations of turbulent flows,[3,4] aeroacoustics,[5,6] electromagnetics,[7,8] and complex unsteady flows,[9,10] the use of higher-order methods is an active area of research. The application of higher-order methods to steady aerodynamic flows has been more limited, despite showing considerable promise.[11–15]

In a previous work by the present authors,[15] a higher-order spatial discretization for the thin-layer Navier-Stokes equations was presented and applied to several turbulent aerodynamic flows. A key feature is that the approximation of the inviscid and viscous fluxes, the numerical boundary schemes, and the numerical integration technique used to calculate forces and moments are all raised to a level of accuracy consistent with global third-order accuracy. The grid convergence studies presented strongly suggest that raising all approximations to comparable accuracy is critical to achieving the benefits of higher-order methods. Subsequent studies[16] confirmed that the fully higher-order discretization is considerably more accurate than the popular approach of using a third-order operator for the inviscid fluxes with a second-order operator for the viscous fluxes.[17,18]

The purpose of the present paper is to further investigate the algorithm presented in the previous work.[15,16] An additional transonic test case is included, and improved grids are used for the transonic cases. The Spalart-Allmaras turbulence model[19] is used for all cases. The paper is organized as follows. After a brief description of the thin-layer Navier-Stokes equations, the higher-order algorithm is presented. The following components are described:

- the discretization of the inviscid flux terms, including the scheme for adding numerical dissipation,
- the discretization of the viscous fluxes,
- the discretization of the turbulence model,
- the treatment of the boundary conditions,
- the integration technique for calculation of forces and moments, and
- the treatment of the left-hand side of the implicit algorithm used to reach steady state.

Test cases and grids are presented next, followed by systematic grid convergence studies[20,21] comparing the accuracy of the higher-order discretization with a well-established second-order discretization. The issue of computational expense is discussed, and convergence histories are compared for all cases. Finally, conclusions and suggestions for future work are presented.

*Graduate Student, stan@oddjob.utias.utoronto.ca
†Professor, Member AIAA, dwz@oddjob.utias.utoronto.ca

## Numerical Method and Governing Equations

The spatial discretizations under study are implemented in ARC2D,[22] developed at the NASA Ames Research Center, which is the basis for the widely used code OVERFLOW.[23] ARC2D uses a generalized curvilinear coordinate system and the diagonal form[24] of the Beam-Warming approximate factorization algorithm[25] with local time stepping to solve the thin-layer Navier-Stokes equations.

In two-dimensional generalized coordinates, the thin-layer Navier-Stokes equations are given by[22]

$$\frac{\partial \widehat{Q}}{\partial t}+\frac{\partial \widehat{E}}{\partial \xi}+\frac{\partial \widehat{F}}{\partial \eta}=\frac{\partial \widehat{S}}{\partial \eta} \tag{1}$$

where $\widehat{Q}=J^{-1}Q=J^{-1}[\rho,\rho u,\rho v,e]^T$ is the vector of conservative dependent variables, $\widehat{E}$ and $\widehat{F}$ are the inviscid flux vectors, $\widehat{S}$ is the viscous flux vector, $\xi$ and $\eta$ are the streamwise and normal generalized coordinates, respectively, and $J$ is the Jacobian of the coordinate transformation.

## Higher-Order Algorithm

With two exceptions (the first-order dissipation added near shock waves and the convective terms in the turbulence model, as discussed below), all approximations in the spatial discretization are consistent with at least third-order global accuracy. The inviscid fluxes are approximated using a fourth-order centered operator plus a third-order matrix dissipation[26] term (first-order at shocks). Note that the popular scalar dissipation scheme[27] is not appropriate for use with a higher-order algorithm, as it introduces far too much error.[28,29] The use of fourth-difference (third-order) dissipation necessitates the use of a five-point stencil and thus the solution of pentadiagonal systems. Increasing the accuracy of the centered difference operator to fourth order does not increase the stencil size, and the overall increase in computing expense per grid node is small. A fourth-order operator is used for the viscous fluxes. Grid metrics are evaluated using the same operators as the convective fluxes without any numerical dissipation. Gustafsson[30] has shown that the numerical boundary schemes can be one order lower than the interior scheme without reducing the global order of accuracy. Hence we can use second-order numerical boundary schemes while preserving third-order global accuracy. Nevertheless, we use third-order boundary schemes wherever possible. Overall, the higher-order algorithm costs roughly 6% more per iteration than a second-order algorithm using the same numerical dissipation scheme.

### Inviscid Fluxes

The following operators are used to approximate first derivatives:

*Interior (4th-order)*

$$\delta_x q_j=\frac{1}{12\Delta x}(-q_{j+2}+8q_{j+1}-8q_{j-1}+q_{j-2}) \tag{2}$$

*First Interior Node (3rd-order)*

$$\delta_x q_j=\frac{1}{6\Delta x}(-2q_{j-1}-3q_j+6q_{j+1}-q_{j+2}) \tag{3}$$

*Boundary (3rd-order)*

$$\delta_x q_j=\frac{1}{24\Delta x}(-11q_j+18q_{j+1}-9q_{j+2}+2q_{j+3}) \tag{4}$$

The last equation is required only for the calculation of grid metrics.

Numerical dissipation is added using matrix dissipation.[26] It requires the same five-point stencil as the fourth-order centered-difference operator and, in the absence of discontinuities, is third-order accurate. The matrix dissipation scheme is implemented in the following manner (An analogous term appears in the $\eta$ direction.):

$$\left(\frac{\partial \widehat{E}}{\partial \xi}\right)_{j,k}\approx \delta_\xi \widehat{E}_{j,k}-\nabla_\xi d_{j+\frac{1}{2},k} \tag{5}$$

with

$$\begin{aligned}
d_{j+\frac{1}{2},k} &= |\widehat{A}|_{j+\frac{1}{2},k}J^{-1}_{j+\frac{1}{2},k}(\epsilon^{(2)}_{j+\frac{1}{2},k}\Delta_\xi Q_{j,k} \\
&\quad -\epsilon^{(4)}_{j+\frac{1}{2},k}\nabla_\xi\Delta_\xi\nabla_\xi Q_{j,k}) \\
\epsilon^{(2)}_{j,k} &= \kappa_2\max(\Upsilon_{j+1,k},\Upsilon_{j,k},\Upsilon_{j-1,k}) \\
\epsilon^{(4)}_{j,k} &= \max(0,\kappa_4-\epsilon^{(2)}_{j,k}) \\
\Upsilon_{j,k} &= \frac{|p_{j+1,k}-2p_{j,k}+p_{j-1,k}|}{|p_{j+1,k}+2p_{j,k}+p_{j-1,k}|}
\end{aligned}$$

where $\delta_\xi$ is the fourth-order centered difference operator given in Eq. 2, $\Delta_\xi$ and $\nabla_\xi$ are first-order forward and backward difference operators, and $\kappa_4=0.02$. We use $\kappa_2=0$ in both directions for subsonic flows, and $\kappa_2=1.0$ in the $\xi$ direction with $\kappa_2=0$ in the $\eta$ direction for transonic flows. The term $\Upsilon_{j,k}$ is a pressure switch to control the use of first-order dissipation near shock waves. The matrix $|\widehat{A}|$ is given by

$$|\widehat{A}|=T_\xi|\Lambda_\xi|T_\xi^{-1} \tag{6}$$

with $|\Lambda_\xi|$ containing the eigenvalues of the flux Jacobian matrix $\widehat{A}=\frac{\partial \widehat{E}}{\partial \widehat{Q}}$, as follows:

$$|\Lambda_\xi|=\begin{bmatrix} |U| & 0 & 0 & 0 \\ 0 & |U| & 0 & 0 \\ 0 & 0 & |U+c\,\theta| & 0 \\ 0 & 0 & 0 & |U-c\,\theta| \end{bmatrix} \tag{7}$$

where $U$ is the contravariant velocity component in the $\xi$ direction, $c$ is the speed of sound, $\theta=\sqrt{\xi_x^2+\xi_y^2}$, and $\xi_x$ and $\xi_y$ are metrics of the curvilinear coordinate transformation. The matrix $T_\xi$ contains the right eigenvectors of $\widehat{A}$. In evaluating $|\widehat{A}|_{j+\frac{1}{2},k}$ we have used the simple average; the Roe average is recommended for flows containing very strong shock waves. To avoid zero eigenvalues, the elements of $|\Lambda|_\xi$ are modified as follows:

$$\begin{aligned}\tilde{\lambda}_1, \tilde{\lambda}_2 &= \max(\lambda_{1,2}, V_l\sigma) \\ \tilde{\lambda}_3 &= \max(\lambda_3, V_n\sigma) \\ \tilde{\lambda}_4 &= \max(\lambda_4, V_n\sigma)\end{aligned} \quad (8)$$

where $\sigma$ is the spectral radius of the flux Jacobian. We use $V_l = V_n = 0$ for subsonic flows, and $V_l = 0.025$, $V_n = 0.25$ for transonic flows. At near-boundary nodes, the following operator is used for the dissipation:

$$\frac{1}{\Delta x}(-q_{j-1} + 3q_j - 3q_{j+1} + q_{j+2}) \quad (9)$$

**Viscous Fluxes**

The viscous terms are in the following general form:

$$\partial_x(\alpha_j \partial_x \beta_j) \quad (10)$$

The following fourth-order expression is used to calculate the $\partial_x \beta_j$ term at half nodes:

$$\begin{aligned}(\delta_x\beta)_{j+\frac{1}{2}} &= \frac{1}{24\Delta x}(\beta_{j-1} - 27\beta_j \\ &\quad +27\beta_{j+1} - \beta_{j+2})\end{aligned} \quad (11)$$

Near boundaries, the following third-order expression is used:

$$\begin{aligned}(\delta_x\beta)_{j+\frac{1}{2}} &= \frac{1}{24\Delta x}(-23\beta_j + 21\beta_{j+1} + 3\beta_{j+2} \\ &\quad -\beta_{j+3})\end{aligned} \quad (12)$$

The value of $\alpha_{j+\frac{1}{2}}$ in Eq. 10 is determined using the following fourth-order interpolation formula:

$$\alpha_{j+\frac{1}{2}} = \frac{1}{16}(-\alpha_{j-1} + 9\alpha_j + 9\alpha_{j+1} - \alpha_{j+2}) \quad (13)$$

Near boundaries, a third-order formula is used:

$$\alpha_{j+\frac{1}{2}} = \frac{1}{8}(3\alpha_j + 6\alpha_{j+1} - \alpha_{j+2}) \quad (14)$$

The complete operator is then:

$$\begin{aligned}\delta_x(\alpha_j\delta_x\beta_j) &= \frac{1}{24\Delta x}[\alpha_{j-3/2}(\delta_x\beta)_{j-3/2} \\ &\quad -27\alpha_{j-1/2}(\delta_x\beta)_{j-1/2} \\ &\quad +27\alpha_{j+1/2}(\delta_x\beta)_{j+1/2} \\ &\quad -\alpha_{j+3/2}(\delta_x\beta)_{j+3/2}]\end{aligned} \quad (15)$$

in the interior, and

$$\begin{aligned}\delta_x(\alpha_j\delta_x\beta_j) &= \frac{1}{24\Delta x}[-23\alpha_{j-1/2}(\delta_x\beta)_{j-1/2} \\ &\quad +21\alpha_{j+1/2}(\delta_x\beta)_{j+1/2} \\ &\quad +3\alpha_{j+3/2}(\delta_x\beta)_{j+3/2} \\ &\quad -\alpha_{j+5/2}(\delta_x\beta)_{j+5/2}]\end{aligned} \quad (16)$$

near boundaries.

**Turbulence Model**

For the Spalart-Allmaras turbulence model, the diffusive terms are handled in the same manner as the viscous terms described in the preceding subsection. A first-order upwind scheme is used for the convective terms in order to maintain positivity of the eddy viscosity. We have experimented with a third-order upwind-biased treatment of the convective terms and seen no degradation in accuracy associated with the use of the first-order operator.

**Boundary Conditions**

The value of $\widehat{Q}$ at a far-field boundary node is calculated as follows:[31]

$$\begin{aligned}\widehat{Q}_{bc} &= \frac{1}{2}(\widehat{Q}_\infty + \widehat{Q}_{ext}) - \frac{1}{2}\mathrm{sign}(\widehat{A})(\widehat{Q}_\infty - \widehat{Q}_{ext}) \\ \mathrm{sign}(\widehat{A}) &= T_\kappa \ \mathrm{sign}(\Lambda_\kappa) \ T_\kappa^{-1}\end{aligned} \quad (17)$$

where $\kappa$ is chosen in the direction normal to the boundary, $bc$ indicates the boundary value, $\infty$ indicates values obtained from free-stream conditions, and $ext$ indicates values extrapolated from the interior nodes of the mesh. The eigenvalues and eigenvectors are calculated from the mean state, $\widehat{Q}_{avg} = \frac{1}{2}(\widehat{Q}_\infty + \widehat{Q}_{ext})$. The following second-order extrapolation operator is used at the far-field boundary:

$$q_j = 3q_{j+1} - 3q_{j+2} + q_{j+3} \quad (18)$$

A far-field circulation correction is also included.[22]

The pressure at the airfoil surface is determined from a third-order approximation to $\partial p/\partial n = 0$, which gives

$$p_1 = \frac{1}{11}(18p_2 - 9p_3 + 2p_4) \quad (19)$$

For an adiabatic wall, $\partial T/\partial n = 0$, and, when coupled with the assumption of zero pressure gradient and the perfect gas law, this implies $\partial\rho/\partial n = 0$. Hence the density at the airfoil surface is determined from an expression analogous to Eq. 19. Note that the assumption that $\partial p/\partial n = 0$ is not strictly correct. However, for aerodynamic flows at high Reynolds numbers, the error introduced is very small. We have experimented with extrapolation of pressure with no significant change in the solution. Furthermore, the error introduced does not depend on the grid spacing, and hence does not affect the conclusions from grid convergence studies. The velocity is zero on the body surface.

For grids with a "C" topology, which are used exclusively in this study, the interpolation at the wake-cut ($wc$) is computed to fourth-order using the data above and below the wake-cut as follows:

$$q_{k_{wc}} = \frac{1}{6}(-q_{k_{wc}+2} + 4q_{k_{wc}+1} + 4q_{k_{wc}-1} - q_{k_{wc}-2}) \quad (20)$$

#### Integration

In order to preserve the accuracy provided by a higher-order solution, it is necessary to use a higher-order integration technique in calculating forces and moments. This is accomplished by fitting a cubic spline to the airfoil coordinates and the surface pressure and skin friction distributions. An adaptive quadrature routine based on the two-point Gauss-Legendre rule with a global error control strategy is then used to perform the integration.[15]

#### Left-Hand Side

The linearization of the right-hand side operator required for the implicit algorithm is carried out such that a pentadiagonal left-hand-side operator is obtained. Since the fourth-order viscous operator described above leads to a seven-point stencil, the standard second-order operator is used on the left-hand side. Approximate linearizations are used for some of the near-boundary operators as well.

## Test Cases and Grids

We consider the following four test cases:

1. NACA 0012 airfoil, $M_\infty = 0.16$, $\alpha = 6°$, $Re = 2.88 \times 10^6$, laminar-turbulent transition at 0.05 and 0.8 chords on the upper and lower surfaces, respectively.

2. NACA 0012 airfoil, $M_\infty = 0.16$, $\alpha = 12°$, $Re = 2.88 \times 10^6$, laminar-turbulent transition at 0.01 and 0.95 chords on the upper and lower surfaces, respectively.

3. NACA 0012 airfoil, $M_\infty = 0.7$, $\alpha = 3°$, $Re = 9.0 \times 10^6$, laminar-turbulent transition at 0.05 chords on both surfaces.

4. RAE 2822 airfoil, $M_\infty = 0.729$, $\alpha = 2.31°$, $Re = 6.5 \times 10^6$, laminar-turbulent transition at 0.03 chords on both surfaces.

These cases span a range of typical aerodynamic flows. Cases 1 and 2 are both subsonic flows, the former fully attached, the latter mildly separated. Experimental data can be found in Gregory and O'Reilly.[33] Cases 3 and 4 are transonic flows with moderate-strength shock waves. Experimental data for Case 4 can be found in Cook et al.[34] The measured coordinates for the RAE 2822 airfoil are used, as in Maksymiuk et al.,[35] rather than the standard coordinates.

Tables 1 and 2 describe the grids used for the subsonic and transonic cases, respectively. All of the grids have a "C" topology. The distance to the far-field boundary is 12 chords for all grids. While this causes some numerical error,[20] it is not a discretization error, and hence will not affect our conclusions. Grid A was generated using an elliptic grid generator. Grid B was generated by removing every second node in both coordinate directions from grid A, and grid C was similarly generated from grid B. This technique produces a sequence of grids suitable for a grid convergence study. The grids for the transonic cases have an increased node density in the normal direction and more nodes on the upper surface than the lower surface (but no clustering at the shock). For both subsonic and transonic cases, grid C is relatively coarse, with a node density suitable for extension to three-dimensional computations, while grids A and B are primarily for estimation of solution error.

## Results and Discussion

In this section, we compare results computed using the higher-order algorithm with those computed using a second-order discretization for both inviscid and viscous fluxes together with matrix dissipation. Zingg at al.[16] showed that this second-order discretization produces numerical accuracy which is very similar to that obtained using either a third-order upwind-biased flux-difference-split scheme or the convective upstream split pressure scheme with second-order approximations for the viscous fluxes. Hence this lower-order discretization is representative of the most popular current algorithms and provides a suitable benchmark for assessing the higher-order discretization. Although errors in drag components associated with laminar-turbulent transition, turbulence, and the thin-layer approximation undoubtedly exceed two percent, one would generally like to reduce numerical errors to below this level, both to permit accurate assessment of physical-model error and to avoid compounding these errors.

Fig. 1 shows the lift, pressure drag, and skin-friction drag computed for case 1 using the higher-order and second-order algorithms on grids A, B, and C. They are plotted versus $1/N$, where $N$ is the number of grid nodes. Agreement between the two algorithms on grid A is good, indicating that numerical errors are very small on this grid. Thus grid A provides a reference for estimating numerical errors on grids B and C. For case 1, both algorithms produce errors in lift of less than one percent on grid C. The errors in pressure drag on grid C are larger, with the higher-order algorithm producing about 3 percent error and the second-order algorithm producing an error in excess of 30 percent. Similarly, the higher-order algorithm produces an error in friction drag below 2 percent on grid C, while the error from the second-order algorithm exceeds 15 percent. Note that these figures provide no evidence that the higher-order algorithm is actually displaying third-order global accuracy. This is probably impossible to achieve without a special treatment of flow and grid singularities. Of more relevance here is the comparison of the errors on grid C, which is typical of grids

| Grid | Dimensions | Points on Airfoil | Off-Wall Spacing ($\times 10^{-6}$) | Leading Edge Clustering ($\times 10^{-3}$) | Trailing Edge Clustering ($\times 10^{-3}$) |
|---|---|---|---|---|---|
| A | $1057 \times 193$ | 801 | 0.23 | 0.1 | 0.5 |
| B | $529 \times 97$ | 401 | 0.53 | 0.2 | 1.0 |
| C | $265 \times 49$ | 201 | 1.2 | 0.4 | 2.0 |

**Table 1 Grids for subsonic cases.**

| Grid | Dimensions | Points on Airfoil | Off-Wall Spacing ($\times 10^{-6}$) | Leading Edge Clustering ($\times 10^{-3}$) | Trailing Edge Clustering ($\times 10^{-3}$) |
|---|---|---|---|---|---|
| A | $1073 \times 257$ | 849 | 0.23 | 0.1 | 0.25 |
| B | $537 \times 129$ | 425 | 0.53 | 0.2 | 0.5 |
| C | $269 \times 65$ | 213 | 1.2 | 0.4 | 1.0 |

**Table 2 Grids for transonic cases.**

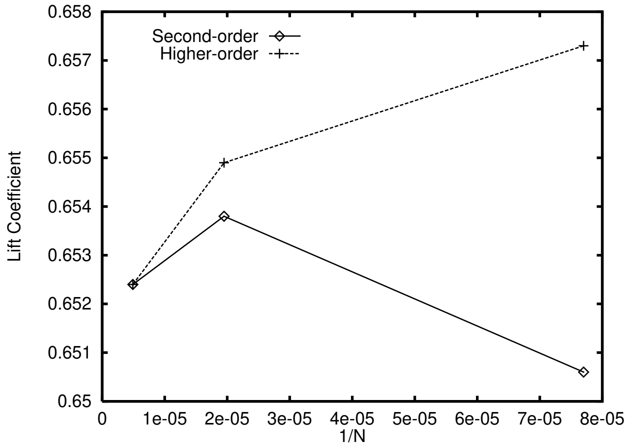


**a)** $C_l$

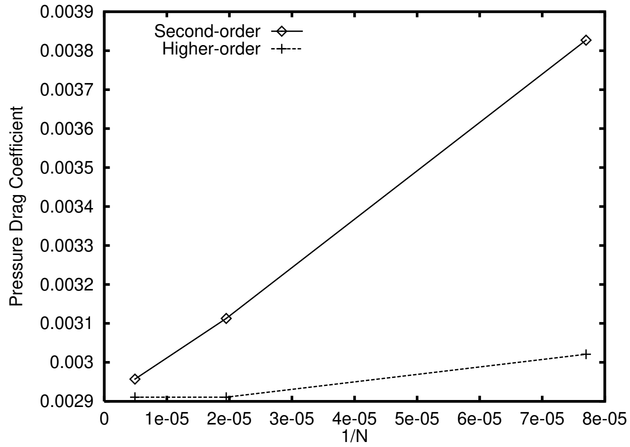


**b)** $C_{d_p}$

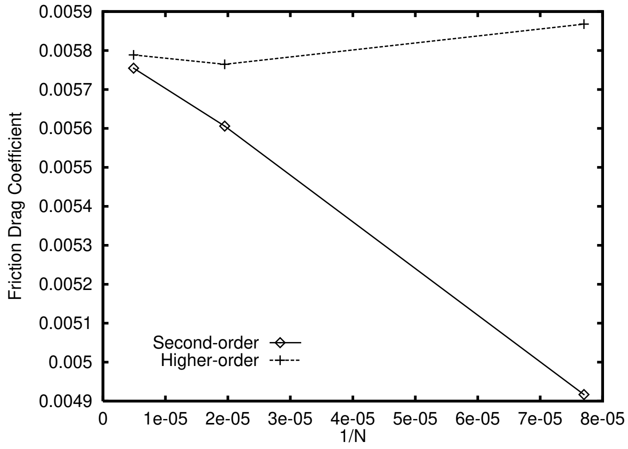


**c)** $C_{d_f}$

**Fig. 1 Grid convergence for Case 1.**

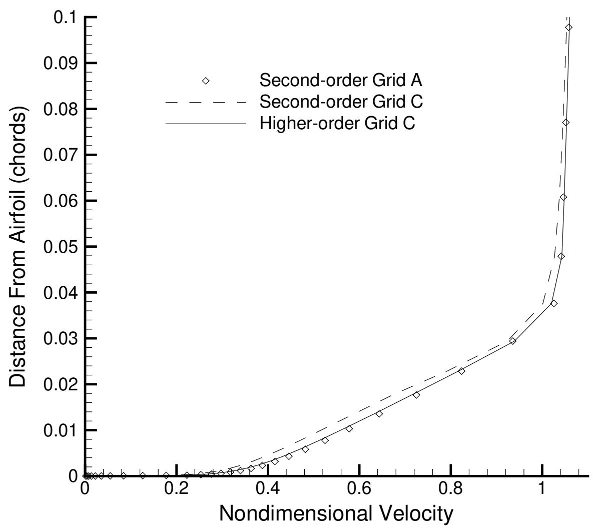


**Fig. 3 Boundary layer velocity profiles on the upper surface at 85% chord, Case 2.**

used in practice. Based on Fig. 1, the higher-order solution computed on grid C is more accurate than the second-order solution computed on grid B, which has four times as many nodes.

Results for case 2, shown in Fig. 2, are similar. The higher-order algorithm produces much smaller errors than the second-order algorithm on grid C. For example, the pressure drag error from the second-order scheme exceeds 30 percent, while that from the higher-order scheme is less than 5 percent. The higher-order algorithm is again more accurate on grid C than the second-order algorithm on grid B. Fig. 3 displays computed boundary-layer velocity profiles on the upper surface near the trailing edge. The symbols show the second-order solution on grid A, which is indistinguishable from the higher-order solution on grid A, with every fourth point plotted. The second-order results computed on grid C are seen to deviate significantly from this reference, while the higher-order solution is nearly grid independent.

Grid convergence studies for the two transonic cases are shown in Figs. 4 and 5. Numerical errors in lift are generally below one precent. The second-order algorithm produces significant errors in the drag components on grid C. The drag components computed using the higher-order algorithm on grid C show very little error and are again more accurate than those computed using the second-order algorithm on grid B. The higher-order results indicate that the first-order numerical dissipation used to prevent oscillations near shocks does not produce significant errors.

The grid convergence studies demonstrate that the higher-order algorithm produces much smaller numerical errors than the second-order algorithm on a given grid. In most cases, the higher-order solutions on grid C are comparable to the second-order solutions computed on grids with four to sixteen times as many nodes. To examine the improvement in efficiency, we must consider the cost of the two algorithms. In terms of memory, there is very little overhead associated with the higher-order algorithm. Therefore, the reduced grid density requirements of the higher-order algorithm translate directly into savings in memory. With respect to computing time, the higher-order algorithm requires roughly six percent more time per iteration. Convergence histories for grid C are displayed in Fig. 6. In all cases, the two algorithms converge similarly for the first three to four orders of magnitude reduction in residual, and the higher-order algorithm converges somewhat more slowly after that. Convergence of lift and drag is typically achieved after about four orders of residual reduction on grid C, so the extra cost associated with the higher-order algorithm is quite small. Therefore, the higher-order algorithm produces solutions of a given accuracy much more efficiently than the second-order algorithm.

## Conclusions

We have presented a stable, accurate, and robust higher-order algorithm for aerodynamic flows, and, furthermore, we have compared its efficiency with that of a well-established second-order algorithm. The primary conclusion is that the higher-order algorithm is much more efficient than the second-order algorithm, requiring substantially fewer grid nodes to reduce numerical errors to desirable levels for both subsonic and transonic flows. A key aspect of the higher-order algorithm is that almost all approximations are raised to a level of accuracy consistent with third-order global accuracy. The two exceptions are the first-order treatment of the convective terms in the Spalart-Allmaras turbulence model and the first-order numerical dissipation added near shocks. It is noteworthy that high accuracy is obtained for transonic cases without clustering the grid near the shocks despite the first-order dissipation used for shock capturing.

This investigation suggests a number of avenues for future work, including the following:

- The largest remaining source of numerical error in the higher-order algorithm should be determined and addressed if practical.
- Further studies should be performed to determine the source of the differences between the solutions computed using the two algorithms on grid A.
- Extension of the higher-order algorithm to three dimensions should be carried out.
- There remains a need for a means of reliably calculating or estimating global solution error.

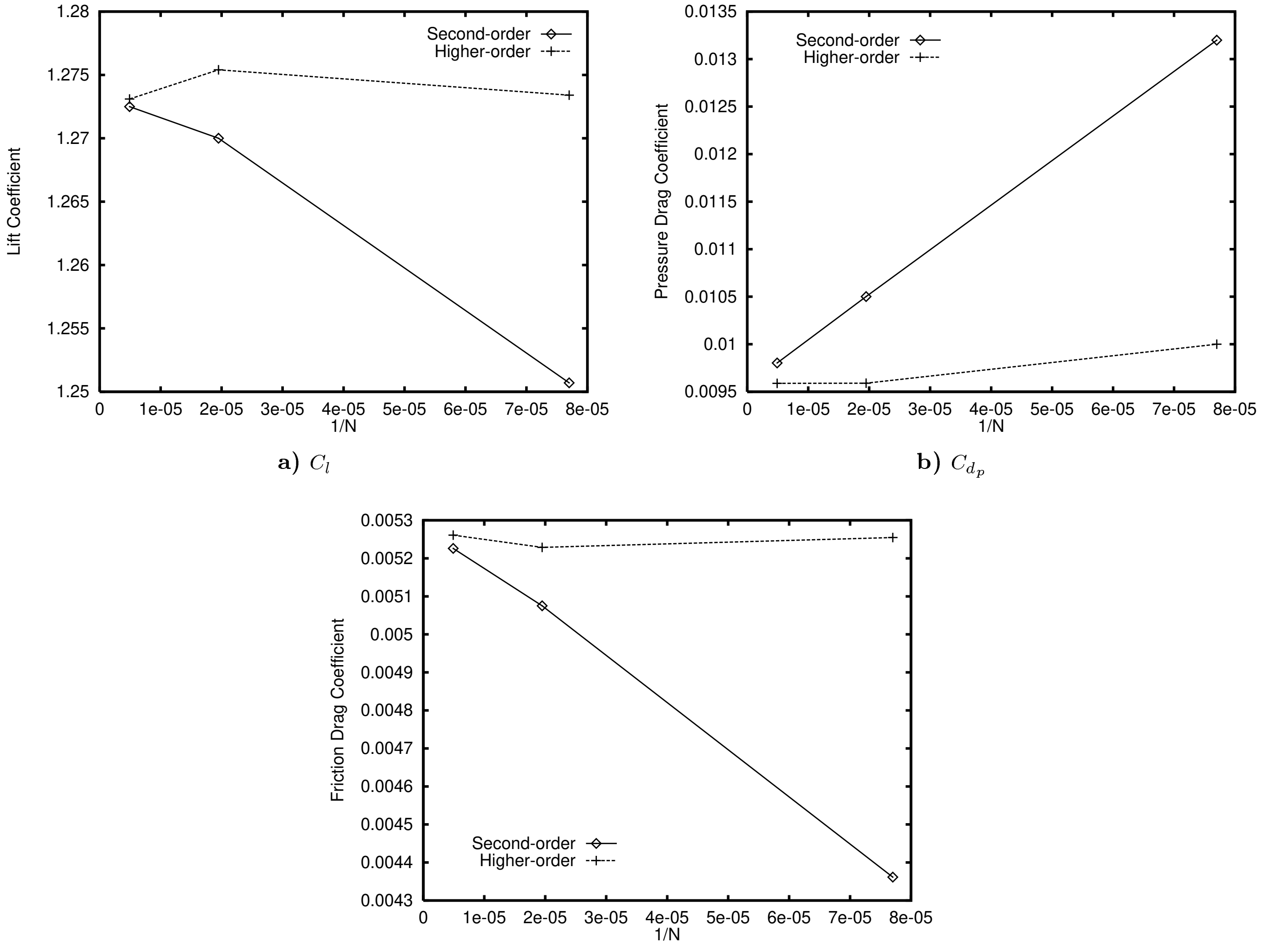


**a)** $C_l$

**b)** $C_{d_p}$

**c)** $C_{d_f}$

**Fig. 2 Grid convergence for Case 2.**

## References


[1]Kreiss, H.-O., and Oliger, J., "Comparison of Accurate Methods for the Integration of Hyperbolic Equations," *Tellus*, vol. 24, 1972, pp. 199–215.

[2]Swartz, B., and Wendroff, B., "The Relative Efficiency of Finite Difference and Finite Element Methods," *Siam J. Num. Anal.*, vol. 11, no. 5, 1974, pp. 979–993.

[3]Rai, M.M., and Moin, P., "Direct Numerical Simulation of Transition and Turbulence in a Spatially Evolving Boundary Layer," *J. Comp. Phys.*, Vol. 109, 1993, pp. 169-192.

[4]Zhong, X., "High-Order Finite-Difference Schemes for Numerical Simulation of Hypersonic Boundary-Layer Transition," *J. Comput. Phys.*, Vol. 144, 1998, pp. 662-709.

[5]Ekaterinis, J.A., "Implicit, High-Resolution, Compact Schemes for Gas Dynamics and Aeroacoustics," *J. Comput. Phys.*, Vol. 156, 1999, pp. 272-299.

[6]Wells, V.L., and Renaut, R.A., "Computing Aerodynamically Generated Noise," in *Annu. Rev. Fluid Mech.*, vol. 29, 1997, pp. 161–199.

[7]Zingg, D.W., Lomax, H., and Jurgens, H.M., "High-Accuracy Finite-Difference Schemes for Linear Wave Propagation," *SIAM J. on Scientific Computing*, Vol. 17, pp. 328-346, March 1996.

[8]Zingg, D.W., "A Review of High-Order and Optimized Finite-Difference Methods for Simulating Linear Wave Phenomena." AIAA Paper 97-2088, June 1997.

[9]Rangwalla, A.A., and Rai, M.M., "A Multi-Zone High-Order Finite-Difference Method for the Navier-Stokes Equations," AIAA Paper 95-1706, June 1995.

[10]Visbal, M.R., and Gaitonde, D.V., "High-Order-Accurate Methods for Complex Unsteady Subsonic Flows," *AIAA J.*, Vol. 37, No. 10, 1999, pp. 1231-1239.

[11]Rigby, D.L., "Compact Spatial Differencing and Subiteration Time Marching in the PARC Code." AIAA Paper 96-0385, January 1996.

[12]Treidler, E.B., and Childs, R.E., "High-Accuracy Spatial Discretization Schemes for CFD," AIAA Paper 97-0541, Jan. 1997.

[13]Treidler, E.B., Ekaterinis, J., and Childs, R.E., "Efficient Solution Algorithms for High-Accuracy Central Difference CFD Schemes," AIAA Paper 99-0302, Jan. 1999.

[14]Rai, M.M., and Chakravarty, S.R., "Conservative High-Order-Accurate Finite-Difference Methods for Curvilinear Grids," AIAA Paper 93-3380, June 1993.

[15]De Rango, S., and Zingg, D.W., "Aerodynamic Computations Using a Higher-Order Algorithm," AIAA Paper 99-0167, Jan. 1999.

[16]Zingg, D.W., and De Rango, S., and Nemec, M., and Pulliam, T.H., "Comparison of Several Discretizations for the Navier-Stokes Equations," AIAA Paper 99-3260, June 1999.

[17]Koren, B. "Upwind Schemes, Multigrid and Defect Correction for the Steady Navier-Stokes Equations" Proc. 11th Int. Conf. on Num. Meth. in Fluid Dynamics, edited by D.L. Dwoyer, M.Y. Hussani, and R.G. Voigt, Springer-Verlag, Berlin, 1989.

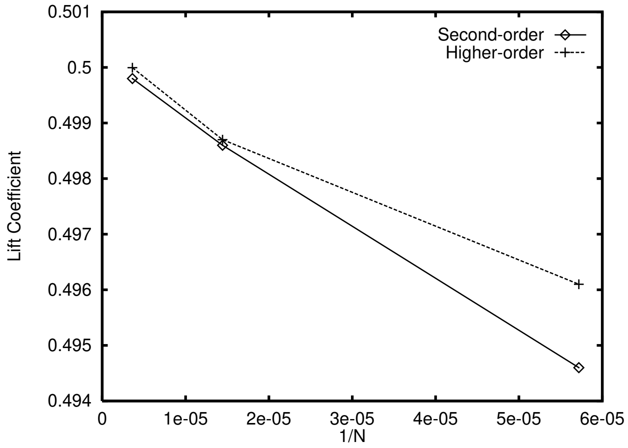


**a)** $C_l$

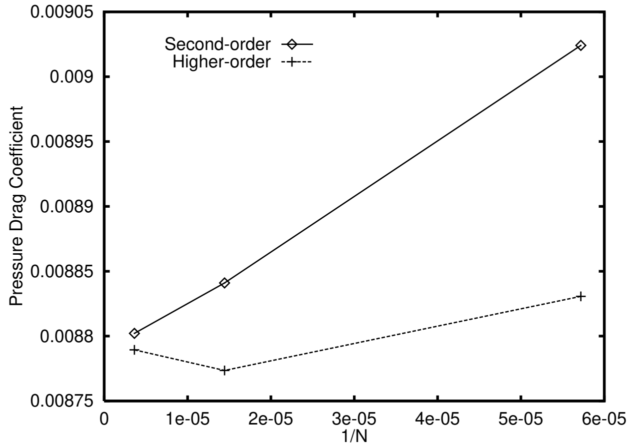


**b)** $C_{d_p}$

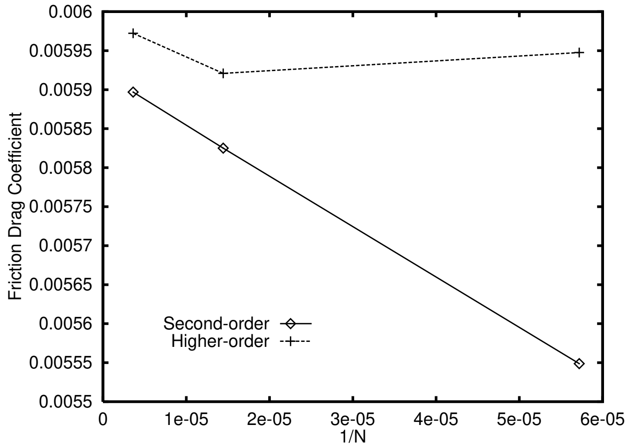


**c)** $C_{d_f}$

**Fig. 4 Grid convergence for Case 3.**


[18] Rai, M.M., "Navier-Stokes Simulations of Rotor-Stator Interaction Using Patched and Overlaid Grids," *AIAA J. of Propulsion and Power*, Vol. 3, No. 5, 1987, pp. 387-396.

[19] Spalart, P. R., and Allmaras, S. R., "A One-Equation Turbulence Model for Aerodynamic Flows." AIAA Paper 92-0439, January 1992.

[20] Zingg, D.W., "Grid Studies for Thin-Layer Navier-Stokes Computations of Airfoil Flowfields," *AIAA J.*, Vol. 30, No. 10, 1992, pp. 2561-2564.

[21] Roache, P.J., *Verification and Validation in Computational Science and Engineering*, Hermosa, New Mexico, 1998.

[22] Pulliam, T.H., "Efficient Solution Methods for the Navier-Stokes Equations," Lecture Notes for the Von Karman Institute for Fluid Dynamics Lecture Series, Brussels, Jan. 1986.

[23] Jespersen, D., Pulliam, T., and Buning, P., "Recent Enhancements to OVERFLOW," AIAA Paper 97-0644, Jan. 1997.

[24] Pulliam, T.H., and Chaussee, D.S., "A Diagonal Form of an Implicit Approximate-Factorization Algorithm," *J. Comp. Phys.*, Vol. 39, 1981, pp. 347-363.

[25] Beam, R., and Warming, R.F., "An Implicit Finite-Difference Algorithm for Hyperbolic Systems in Conservation Law Form," *J. Comp. Phys.*, Vol. 22, 1976, pp. 87-110.

[26] Swanson, R.C., and Turkel, E., "On Central-Difference and Upwind Schemes," *J. Comp. Phys.*, Vol. 101, 1992, pp. 292-306.

[27] Jameson, A., Schmidt, W., and Turkel, E., "Numerical Solutions of the Euler Equations by Finite Volume Methods Using Runge-Kutta Time Stepping," AIAA Paper 81-1259, June 1981.

[28] Allmaras, S.R., "Contamination of Laminar Boundary Layers by Artificial Dissipation in Navier-Stokes Solutions," *Numerical Methods for Fluid Dynamics*, edited by M.J. Baines and K.W. Morton, Clarendon, Oxford, UK, 1993.

[29] Frew, K., Zingg, D.W., and De Rango, S., "Artificial Dissipation Schemes for Viscous Airfoil Computations," AIAA J., Vol. 36, No. 9, Sept. 1998, pp. 1732-1734.

[30] Gustafsson, B., "The Convergence Rate for Difference Approximations to Mixed Initial Boundary Value Problems," *Math. Comp.*, vol. 29, no. 130, pp. 396–406, 1975.

[31] Barth, T.J., "Aspects of Unstructured Grids and Finite-Volume Solvers for the Euler and Navier-Stokes Equations," Lecture Notes for the Von Karman Institute for Fluid Dynamics Lecture Series, 1994-05, Brussels, 1994.

[32] Malcolm, M.A., and Simpson, R.B., "Local Versus Global Strategies for Adaptive Quadrature." ACM Transactions on Mathematical Software, Vol. 1, No. 2, June 1975.

[33] Gregory, N., and O'Reilly, C.L., "Low-Speed Aerodynamic Characteristics of NACA 0012 Airfoil Section, Including the Effects of Upper-Surface Roughness Simulating Hoar Frost," Aeronautical Research Council, Reports and Memoranda No. 3726, U.K., Jan. 1970.

[34] Cook, P.H., MacDonald, M.A., and Firmin, M.C.P., "Aerofoil RAE 2822 - Pressure Distributions, and Boundary-Layer and Wake Measurements," AGARD-AR-138, May 1979.

[35] Maksymiuk, C.M., Swanson, R.C., and Pulliam, T.H., "A Comparison of Two Central Difference Schemes for Solving the Navier-Stokes Equations," NASA TM-102815, July 1990.

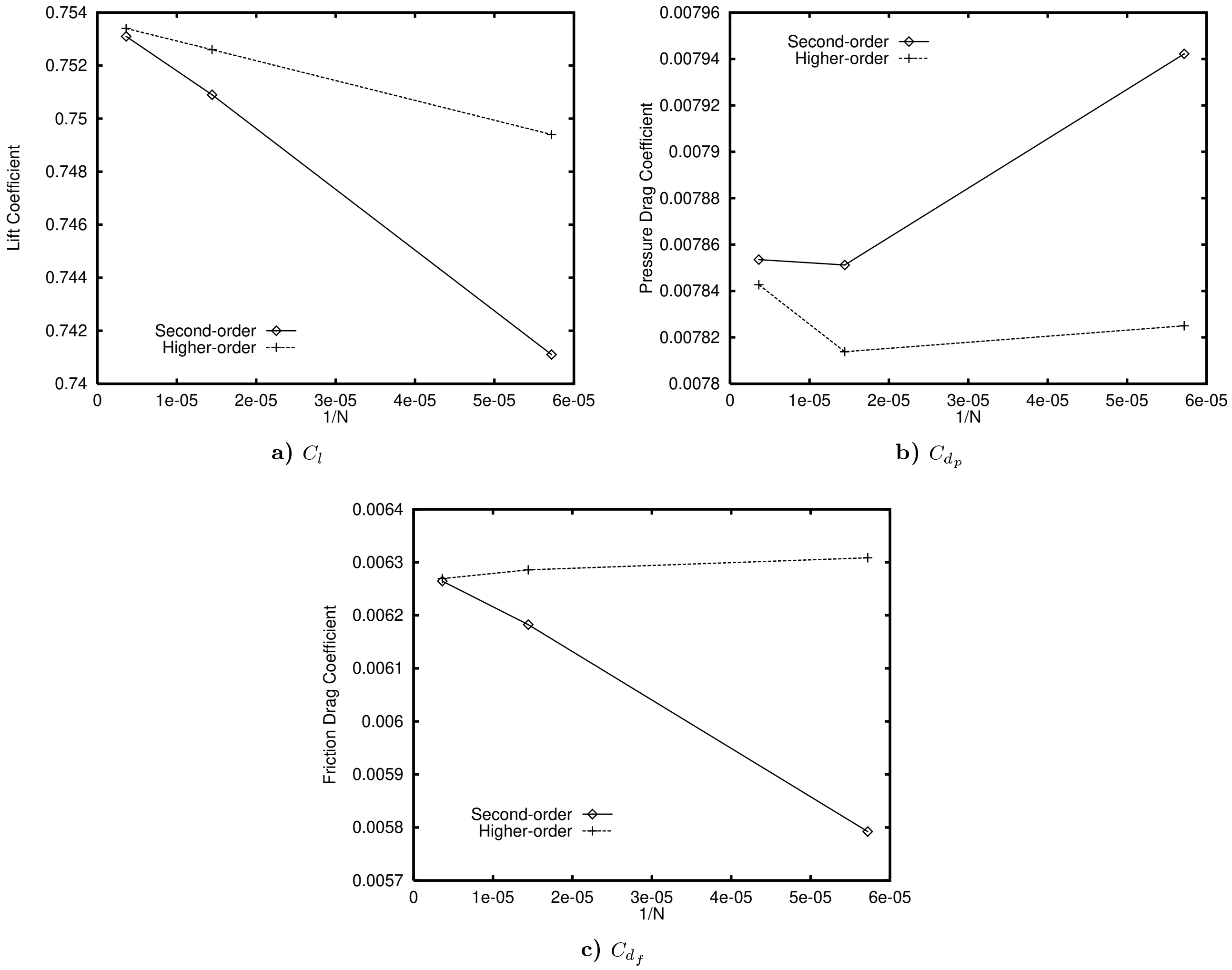


**a)** $C_l$

**b)** $C_{d_p}$

**c)** $C_{d_f}$

**Fig. 5 Grid convergence for case 4.**

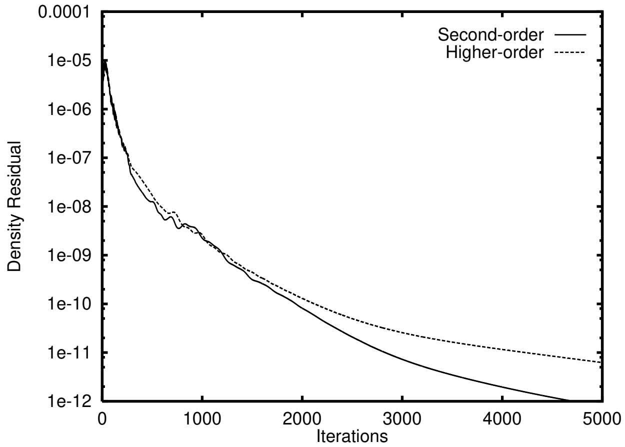


**a)** Case 1

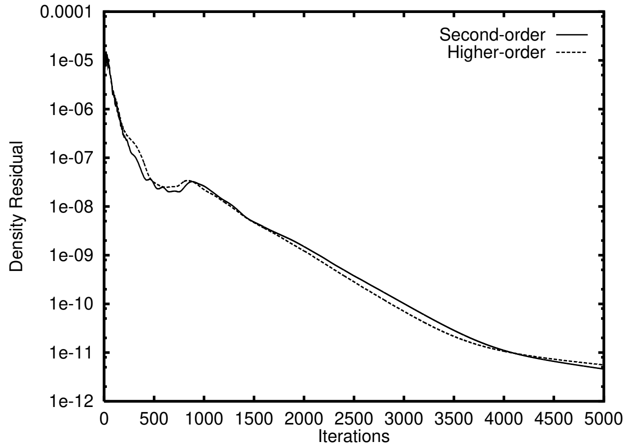


**b)** Case 2

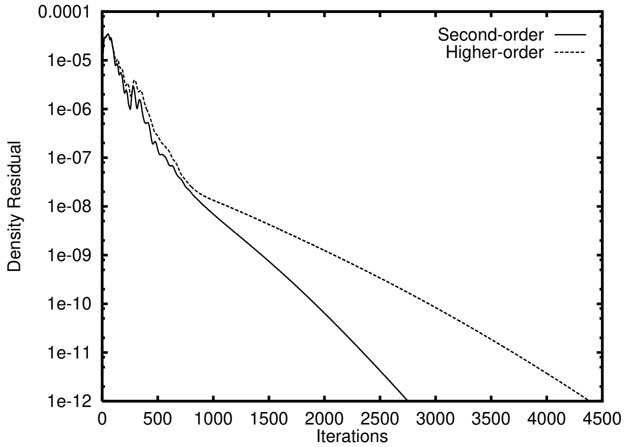


**c)** Case 3

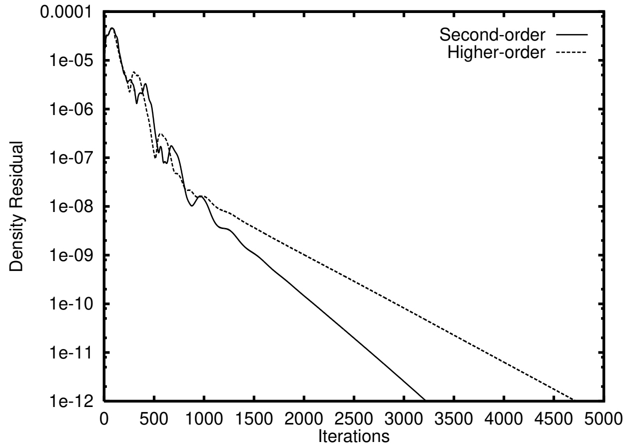


**d)** Case 4

**Fig. 6 Residual histories on grid C.**